Development of actual powder layer height depending on nominal layer thicknesses and selection of laser parameters

Deniz Jansen[ab], Theresa Hanemann[ac*], Markus Radek[a], Astrid Rota[a], Jörg Schröpfer[b], Martin Heilmaier[c]

[a]EOS Electro Optical Systems GmbH, Krailling, Germany

[b]University of Applied Sciences, Munich, Germany

[c]Institute of Applied Materials (IAM-WK), Karlsruhe Institute of Technology (KIT), Karlsruhe, Germany

[*]Corresponding author, E-Mail: theresa.hanemann@eos.info

Abstract

For an improved understanding and modelling of the melting process and dynamics in laser powder bed fusion the knowledge of the actual powder layer height and its development is essential. According to theoretical calculations the powder layer thickness approaches the quotient of the nominal layer height and the powder layer density after several layers. However, a previous study shows that in this stable state the actual powder layer thickness is much higher than theoretically expected due to denudation and spattering. Based on the approach of past investigations this study examines experimentally the development of the effective powder layer height by varying the nominal layer thickness and the laser parameters. Furthermore, the influence of these process parameters on the formation of the denudation zone was examined. The results show the significant impact of the variation of the laser parameters on the actual powder layer thickness likely caused by denudation and spatter effects. Moreover, for low nominal layer heights the effective powder layer thickness is relatively higher. This development seems to be affected by the selection of the laser parameters. The outcomes also provide a possible explanation for the

unexpected high increase in powder consumption, which amounts to at least 98% compared to theoretical calculations within the experiments.

Keywords: Additive Manufacturing, Laser powder bed fusion, Powder layer thickness, Process parameters

1. Introduction

Direct Metal Laser Sintering (DMLS) is an additive manufacturing process and belongs to the family of laser powder bed fusion. It generates three-dimensional parts with high density and quality by layer-wise selective laser melting of powder (Gebhardt and Hötter, 2016). Besides laser power, scan speed and hatch distance, layer thickness represents an essential processing parameter. Therefore, the influence of layer thickness on melt pool morphology and mechanical properties of parts is widely investigated in literature. Yadroitsev and Smurov (2010) varied the layer thickness of single scan lines of 316L fabricated with various scan speeds and laser powers in the range of 0 – 400 µm using a tilted baseplate. They found a critical layer thickness for single track stability, which shifted to higher layer thicknesses with increasing energy input. A similar experiment using a tilted substrate was also used by Li et al. (2012) to investigate the balling behavior of stainless steel and pure nickel powder. Severity of the balling effect was observed to increase for increasing layer thicknesses with additional porosity formation observed for the nickel powder. In addition to stability, Yang et al. (2016) investigated the influence of layer thickness on single line scan dimensions and part mechanical properties of Ti6Al4V fabricated with varying layer thickness from 20 – 60 µm at different laser power and speed combinations. They found layer thickness to be the major influencing factor for melt pool height and a minor influencing factor for melt pool depth, width, and mode, with melt pool mode determining the mechanical properties of parts. The microstructure

and mechanical properties of samples build with different layer thicknesses was also compared for Inconel 718 by Sufiiarov et al. (2017) and maraging steel by Shamsdini et al. (2020). While Suffiiarov et al. (2017) observed a decrease of mechanical properties with increase in layer thickness due to lack-of-fusion porosity, Shamsdini et al. (2020) could not observe a significant deterioration and concluded that higher layer thicknesses can be beneficial for process efficiency if the energy input is kept appropriate to form stable melt pools. Increasing the layer thickness is of special interest as recoating time has a major contribution to the overall production time in DMLS. De Souza et al. (2019) showed that production time for maraging steel could be decreased by 40% with an increase in layer thickness by 66% corresponding to a maximum layer thickness of 75 µm. The study of Leicht et al. (2021) also shows for parts manufactured from 316L a significantly improved productivity with acceptable mechanical properties due to an increase of the layer thickness from 20 µm to 80 µm with adapted energy density. Extending the process window to even higher layer thicknesses Ma et al. (2015) investigated the microstructure and mechanical properties of 1Cr18Ni9Ti samples fabricated with layer thicknesses up to 150 µm at high laser power. However, samples fabricated with the highest layer thicknesses showed the lowest strengths, which was attributed to the formation of porosity. A reduction in density as well as the loss of dimensional accuracy of additively manufactured components when the layer thickness is increased is also observed by Nguyen et al. (2018) who investigated parts manufactured from Inconel 718 with various layer thicknesses of 20 µm, 30 µm, 40 µm and 50 µm. The presented literature can be separated in two methodologies in studying the influence of layer thickness, single line scans and multilayer parts. Although both demonstrate that layer thickness is important in determining the necessary energy input to achieve firm bonding between layers one must be careful with a direct transfer of results.

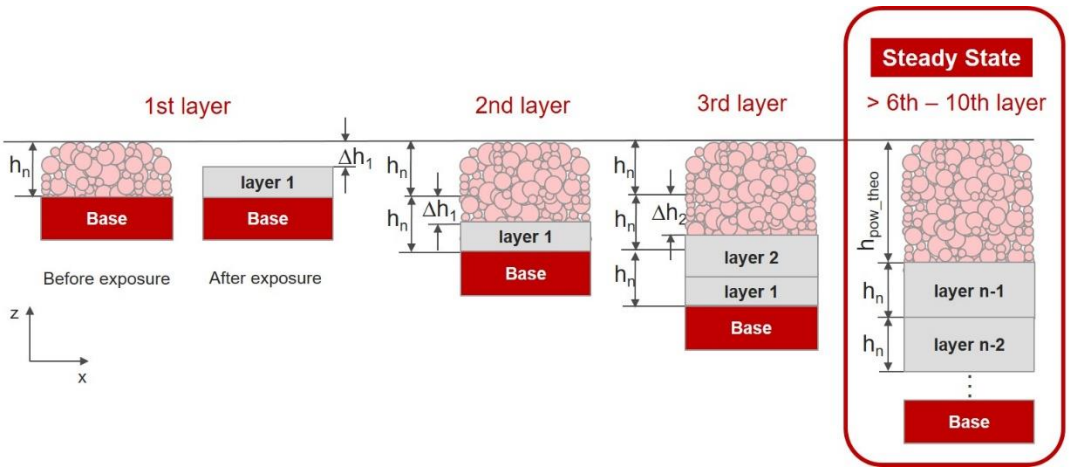

Fig. 1: Schematic of the development of powder layer height without the influence of spatter and denudation, based on Wischeropp et al. (2019)

Regarding the effect of powder layer thickness two different layer thicknesses have to be distinguished: The actual or effective powder layer height, which is defined as the thickness of the newly coated powder layer above a solid part and the nominal layer thickness which describes the leveling height of the building platform and is defined by the user before the building process. Due to consolidation of the powder material during melting, the effective powder layer height deviates from the nominal layer thickness after the first layer. Thus, the nominal layer thickness stated in multilayer experiments as reference is different from the effective powder layer height stated for single line experiments. As the nominal layer thickness is set constant throughout the build process the occurring volume reduction leads to an increase in height of the following powder layer in the first layers (Fig. 1). As the actual height of one melted single layer, the effective melting layer height h_l, approaches the nominal layer thickness h_n a steady state is reached. According to theoretical considerations of Mindt et al. (2016) and Meiners (1999) the powder layer thickness approaches a constant value of the quotient of nominal layer thickness h_n and powder layer density a:

$$h_{pow\_theo,i} = h_n \sum_{k=0}^{i-1}(1-a)^k \quad \xrightarrow{i\to\infty} \quad h_{pow\_theo} = h_n / a \qquad \text{(Eq. 1)}$$

This means that the stable state powder layer thickness depends on the powder layer density. At a powder layer density of 50% the theoretical powder layer height $h_{pow,theo}$ is about twice the nominal height h_n. Spierings and Levy (2009) used Eq. 1 to rationalize their results for relative density of samples printed with 316L powders of different particle size distributions and packing densities of 57.6% to 60.1% from measured tap densities.

The packing density of a single powder layer varies from the powder bed density as the wall effect for layer thicknesses close to the powder particle size increases (Karapatis et al., 1999). Up to 15% lower densities were measured for a single powder layer of 500 µm compared to a bulk powder bed with similar size distribution by Karapartis et al. 1999. The packing density of a single powder layer over varying recoater gap sizes was simulated by Mindt et al. (2016) and results showed an increase in packing density with increasing gap height which saturated to about 50% for a gap size of 200 µm, which is in the range of the calculated bulk powder bed density of 50 – 55%. The simulated powder had a Gaussian particle size distribution of 15 – 70 µm. Single powder layer densities were also measured experimentally by Wischeropp et al. (2019) for 17-4 PH and Ti6Al4V at nominal layer thicknesses of 30 µm and 50 µm. The resulting densities ranged from 44% to 56%. Thus, one could assume a powder layer density of 50% a good estimate for the calculation of the effective powder layer height.

However, additional experiments of Wischeropp et al. (2019) indicated that in steady state processing conditions the actual powder layer height h_{pow} is higher than h_{pow_theo} even when considering the experimental powder layer density. Wischeropp et al. (2019) studied the effective powder layer height of two different powder materials and two nominal layer thicknesses and found effective powder layer thicknesses in range

of 4 - 5.5 times the nominal layer thickness. They assumed that the increase of powder layer height $h_{pow,x}$ resulted out of spatter and denudation effects:

$$h_{pow} = h_{pow\_theo} + h_{pow,x} \quad \text{(Eq. 2)}$$

By these phenomena occurring during exposure, powder particles are deposited away from the melt area and do not belong to the melted material. Therefore, the height of the melted layer is reduced, and the powder layer height increases until steady state is reached. In accordance with the results of Wischeropp et al. (2019), Mahmoodkhani et al. (2019) measured an effective layer thickness of 150 µm for 17-4 PH which is 7.5 times the nominal layer thickness of 20 µm. The evolution of effective powder layer height and melted layer height over several layers was evaluated by Bidare et al. (2017) for 316L with a nominal layer thickness of 40 µm. Steady state with a melted layer height of 40 µm and an effective layer thickness of 133 µm was reached after 10 layers, which amounts to 3.3 times the nominal layer thickness.

While Bidare et al. (2017) and Mahmoodkani et al. (2019) do not explain the increase in effective layer thickness compared to theoretical considerations, Wischeropp et al. (2019) attributed the increase to relocated powder by spatter and denudation not contributing to the melted material. The formation of spatter and denudation for different processing conditions was observed by Bidare et al. (2018) using high speed video recordings as well as Schlieren imaging. They found that powder particles were drawn towards the melt pool by the vapor plume formed from evaporating material and were either entrained in the melt pool or ejected along the plume. Additionally, the powder was also found to be blown away by the impinging vapor plume for fast scan speeds. An overview of the mechanisms behind spatter generation and powder entrainment is given by Ly et al. (2017). It is proposed that

85% of all spatter is generated from powder entrainment and only 15% from recoil pressure driven melt ejection. This emphasizes the important contribution of spatter to the delocalization of powder. The influence of chamber pressure and laser power on denudation by powder entrainment was investigated by Matthews et al. (2016). Denudation zone increased with increasing power, while it was almost unaffected by speed, with a tendency for less denudation at lower speeds. The dependence on chamber pressure was observed to be more complex involving different physical mechanisms for different pressure ranges. The main cause for denudation under pressures typical in commercial LPBF systems was entrainment of powder particles by the vapor plume.

Those studies show that effective powder layer thickness cannot be easily calculated from theoretical estimations and specific process conditions have to be taken into account. However, the knowledge of the actual powder layer height is important for understanding and modelling the laser-powder-interaction as emphasized by Mahmoodkhani et al. (2019) comparing calculated melt pool dimensions for simulations with nominal and effective powder layer thickness. Furthermore, knowledge of the effective layer thickness can help to understand the difference between single layer and multilayer experiments. Therefore, this study represents an extension of the previous research by examining the influence of different laser parameters and nominal layer thicknesses on the formation of the effective powder layer height. The aim is to obtain new insights on the significance of those two factors on effective powder layer height as well as receiving new findings on powder consumption.

2. Experimental procedure

2.1 Characterization of powder material

All samples used fresh IN718 powder (EN 2.4668) from the same batch provided by EOS GmbH. To characterize the properties of the selected powder, its particle size distribution was determined by dry measurement with a Particle Analyser Camsizer XT (Retsch Technology). The powder analysis was performed twice to ensure the results.

2.2. Sample geometry

For investigation of the effective powder layer thickness all experiments were based on the same approach. Just individual process parameters were changed. Fig. 2 illustrates the sample geometry. This geometry was manufactured on a building

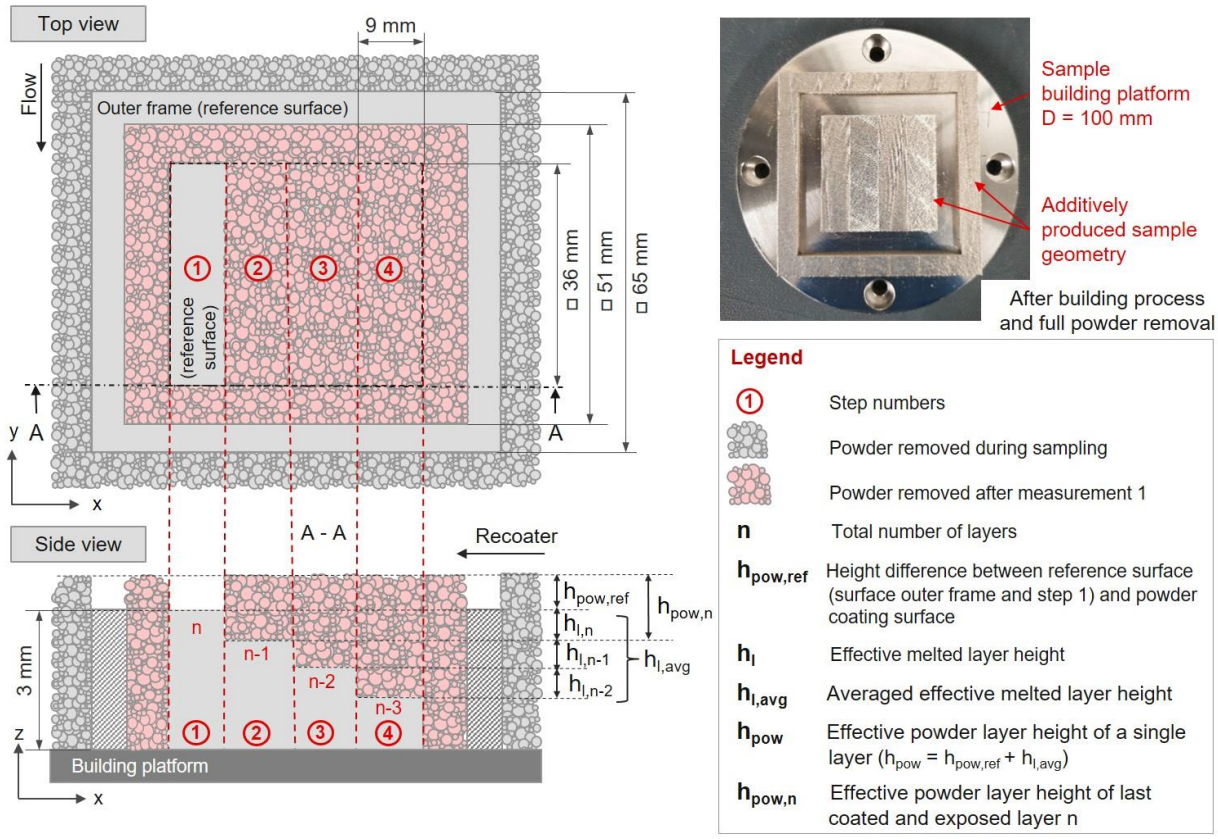

Fig. 2: Dimensions and application of the sample geometry

platform with a diameter of 100 mm. The sample geometry was composed of a central stepped area and an outer frame. Its size in x-y-plane corresponds to the available building platform surface to obtain the largest possible measurement area. The steady state is assumed to be reached, when the total height of the sample amounts to 3 mm corresponding to at least 37 layers. Thus, the limit layer number of 6 to 10 to reach steady state according to Mind et al. (2016) is clearly crossed (Fig. 1). For measuring the height of a single melt layer and to check if steady state is obtained, the height of the integrated steps is equal to the adjusted nominal layer thickness h_n in the virtual model which is transferred to the machine. In addition, the outer frame was integrated to avoid particles trickling away during removal and measurement of the sample.

2.3. Sample generation, measurement and evaluation

In virtual test preparation, the digital sample geometry is centrally placed on the building platform and the process parameters are defined. Then the machine is prepared. After finishing the build process and a cooling time of 30 min, the sample is removed carefully. Thereby, the powder inside the outer frame remained unaffected. Before the entire powder sample was measured using a 3D-profilometer Keyence VR 3200 in macro-setting, the remaining few particles on the last melted layer surfaces of the outer frame and the left step were removed carefully with a brush without affecting the inside powder bed. For the evaluation, these last melted surfaces are defined as reference surfaces. Several profile measurements in x-y-plane, see Fig. 3, are performed to measure the whole sample area. Only the center regions of the profiles for large powder areas are considered when measuring the powder layer thickness to avoid superelevation at the border between powder and sample regions. The evaluation range of the profile measurements remains unchanged for all

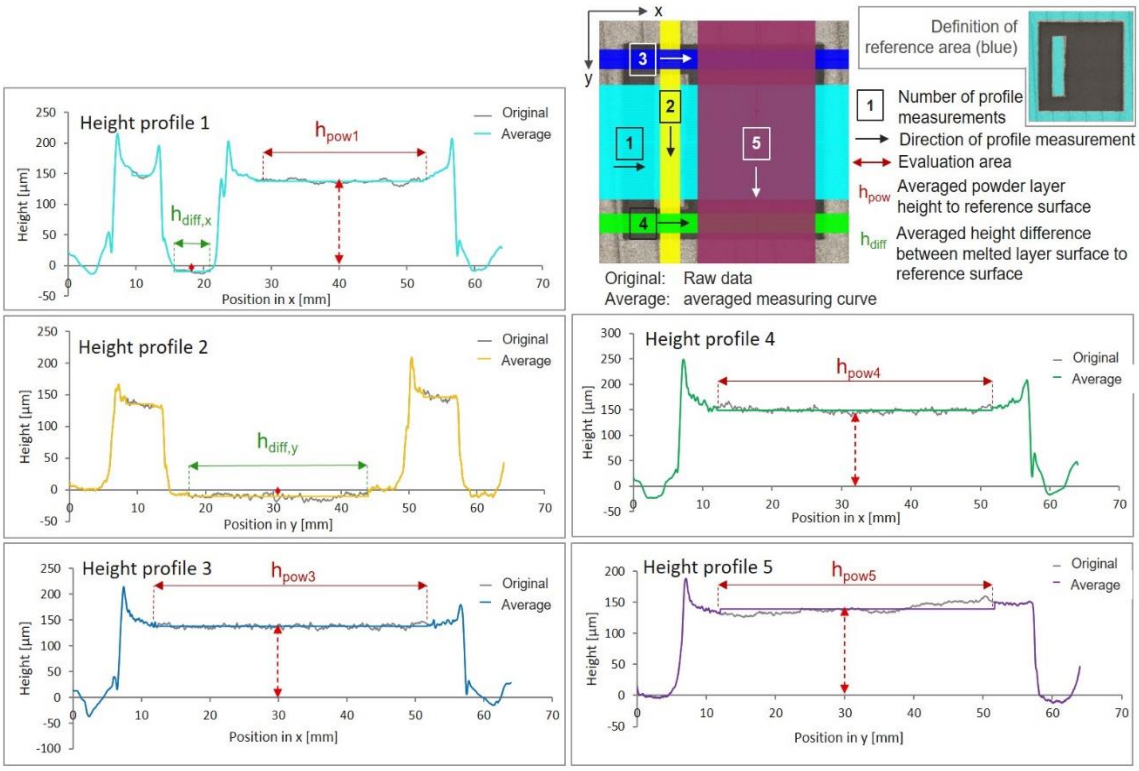

Fig. 3: Example evaluation of a powder sample to determine the effective powder layer height to reference surface $h_{pow,ref}$

samples. The powder height to the reference surface is averaged from the mean height of the several profile measurements h_{pow1}, h_{pow3}, h_{pow4} and h_{pow5} (Fig. 3). In addition, the height difference between the reference plane and the last exposed step is determined and considered as correction factor. Thus, $h_{pow,ref}$ can be calculated as:

$$h_{pow,ref} = ¼ (h_{pow1} + h_{pow3} + h_{pow4} + h_{pow5}) - ½ (h_{diff,x} + h_{diff,y}) \qquad \text{(Eq. 3)}$$

For the second measurement, all powder is removed. The sample is measured in macro-setting again. The last exposed surfaces, the border area and the left step are defined as reference surfaces. The melted steps are measured vertically and horizontally in x-y-plane, see Fig. 4. To obtain the effective single melted layer height h_l of the sample the height difference between adjacent melted steps is calculated and averaged. By these two values the effective powder layer thickness of the sample can be calculated:

$$h_{pow} = h_{pow,ref} + h_l \qquad \text{(Eq. 4)}$$

For describing the relation between effective powder layer height hpow and the nominal layer thickness h_n the factor *F* is defined as follows:

$$F = h_{pow} / h_n \qquad \text{(Eq. 5)}$$

2.4. Examined parameters

To examine the actual layer height for the standard EOS IN718 process three samples with a nominal layer thickness h_n of 40 µm and the recommended laser parameters (basic parameter set) were produced using an EOS M 290 system. The laser spot diameter for the used system was measured to 78 µm with a Primes FocusMonitor FMW+ and the 86.5 % power aperture method (International Organization for Standardization, 2004). To investigate the development of the actual powder layer height depending on nominal layer thickness h_n additional samples with a nominal layer thickness of 10 µm, 20 µm, 30 µm, 60 µm and 80 µm were manufactured with the standard parameter set as well as one additional parameter set of higher energy input *L2* (Table 1). For this purpose, the step height of the sample geometry was virtually adapted to the selected nominal layer thickness in process preparation.

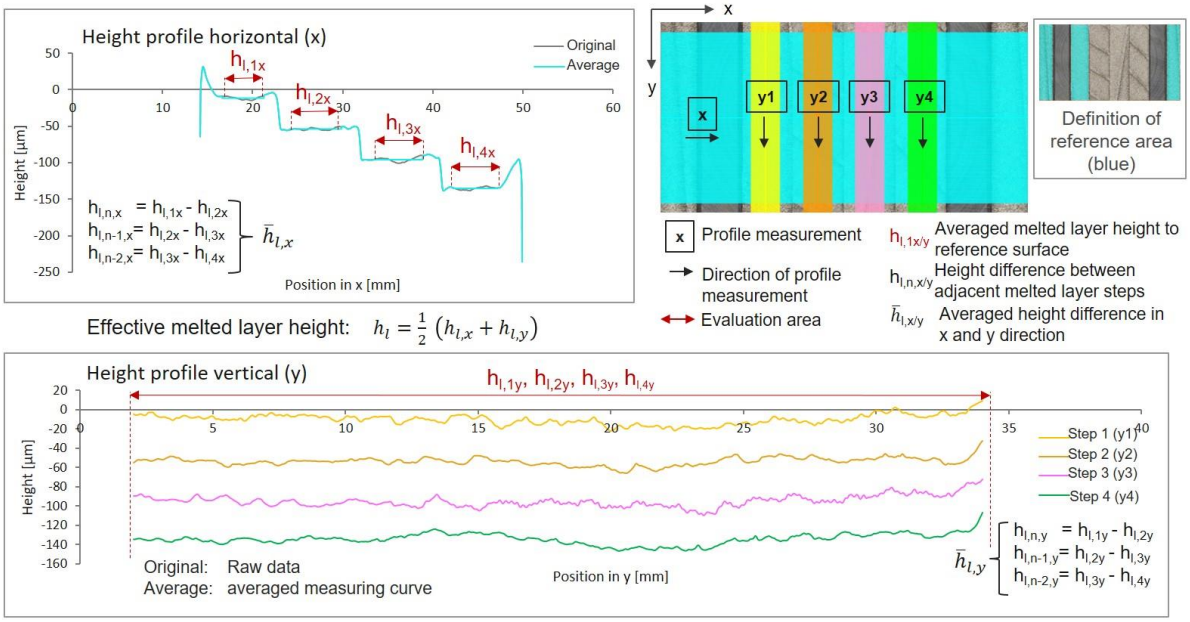

Fig. 4: Example evaluation of a sample without powder to determine the effective melting layer height

Furthermore, the influence of the laser parameters was studied by varying laser power *P* and scan speed *v* (Table 1). For each parameter set one sample with nominal layer thickness of 40 µm was considered. These parameter sets have been examined for their stability and buildability within single track, single layer, and three-dimensional geometry experiments before. In addition, samples with multiple coating and varying dose factors were considered (Table 2). For this purpose, the basic laser parameter set was used. The exposure followed, after reaching a total layer application of 40 µm through multiple coating depending on the selected nominal layer thickness.

Table 1: Laser parameter variation experiment – varied parameters

Set	Laser power *P* [W]	Scan speed *v* [mm/s]	Hatch distance h_a [mm]
L1	200 (↓)	960 (→)	0.096 (↓)
L2	330 (↑)	750 (↓)	0.117 (↑)
L3	200 (↓)	280 (↓)	0.158 (↑)

Comparison to basic parameter set:
↑ higher, ↓ lower, → approximately equal

Table 2: Multiple coating experiment – varied parameters

Set	Number of coatings before exposure	Nominal layer thickness h_n [µm]	Dose factor [%]
M1	2	20	100
M2	2	20	200
M3	4	10	170

2.5. Investigation of powder particle size distribution in the processing chamber

Any change in powder particle size distribution in the process area can lead to a different density and therefore it can affect the effective layer thickness. To investigate this factor cuboids with dimensions 65x65x2.8 mm and the nominal layer thickness h_n of 10 µm and 80 µm were manufactured. After the building process was finished an additional powder layer was applied. The powder lying on the produced

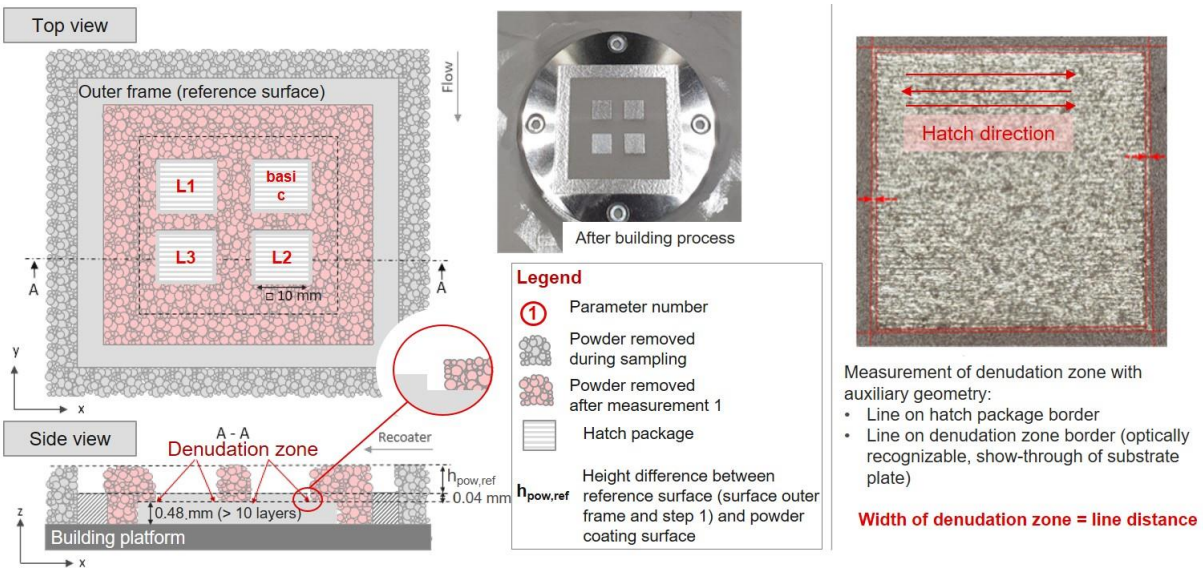

Fig. 5: Experimental setup: Investigation of the influence of laser parameters on the formation of the denudation zone

cuboid as well as powder samples from the dispenser and the powder bed are taken and measured with the Particle Analyser Camsizer XT.

2.6. Investigation of the denudation zone

Besides spattering, the formation of the denudation zone has a significant impact on the effective powder layer thickness of the respective process. This process effect is influenced by the selection of laser parameters. To investigate this behavior and its impact on the effective powder layer thickness four hatch packages with the dimensions 10x10 mm and different parameter sets were manufactured on a similar geometry as shown in Fig. 5. A consistent nominal layer thickness h_n of 40 µm was used. The parameter sets in which the values of laser power and scan speed were varied are listed in Table 1. As in the previous experiments the specimen was carefully removed from the machine including the powder lying on the sample geometry. Based on measurement of this sample with a 3D-profilometer the width of the denudation zone around the hatch packages was determined (Fig. 5). Additionally, the development of the denudation zone by variation of the nominal layer thickness was examined. The experimental procedure was related to the

previous denudation investigation. The sample has four different sections. Each section was built up with the respective nominal layer thickness h_n (10 µm, 20 µm, 40 µm, 80 µm) using multiple coating of 10 µm layers and the basic parameter set. The sample removal and the measurement of the denudation zone remained unchanged.

3. Results and Discussion

3.1. Particle size distribution

Fig. 6 shows the determined particle size distribution of the IN718 powder. It results in a *D10* of 18 µm, a *D90* of 49 µm and a *D50* of 32 µm. Thus, the particle size distribution for the used powder lies within a typical range for LPBF powders which is stated as 10 µm to 60 µm in Vock et al. (2019). Table 3 lists further powder density properties. The measured relative powder bed density for the used IN718 powder of about 54% is in good agreement with the powder bed density of 55.8 ± 6.44% obtained by Ali et al. (2018) for *Hasteloy X* with a similar powder size range at the center region of an *EOS M 290* build chamber.

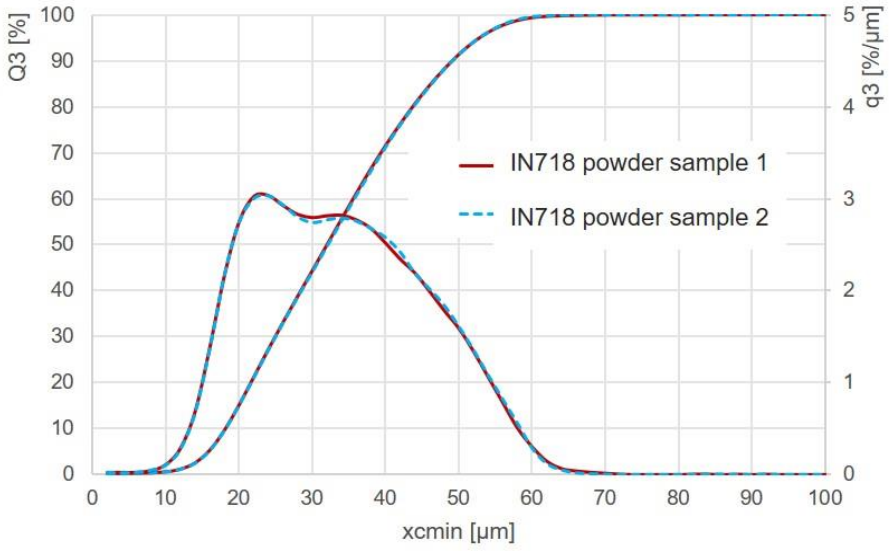

Fig. 6: Particle size distribution of used IN718 powder

Table 3: Summary of powder and processing properties of used IN718 powder

Particle size distribution	
D10	18 µm
D50	32 µm
D90	49 µm
Density	
Material density (EOS,2011)	min. 8.15 g/cm³
Powder bed density*	4.40 g/cm³

* experimentally determined according to the method from (Kurzlechner, 2016)

3.2. Effective powder layer thickness of the 40-µm-process

The effective layer thickness and the molten layer height of three samples manufactured with a nominal thickness of 40 µm and the basic laser parameter set was measured. The average height of one single molten layer amounts to 43 ± 8 µm. Thus, the mean of the effective melted layer height h_l is only marginally higher than the adjusted nominal layer thickness and lies within the positioning accuracy of the machine axis. This shows that steady state has been reached. With a value of 191 ± 13 µm, the effective powder layer height h_{pow} is 4.5 times higher than the determined effective melted layer height h_l and 4.8 times the nominal layer thickness h_n. The obtained factors are in the range of the results of Wischeropp et al. (2019). With the experimentally determined powder bed density of 4.40 g/cm³ and the material density of 8.15 g/cm³ (Table 3), the relative powder bed density a_p can be calculated to a_p = 0.54. Although the powder layer density of a thin layer might be different from the powder bed density as discussed in the introduction, the gap height between the recoater and the solidified layer which equals the effective powder layer height is more than three times the *D90* of the used powder and thus the layer density can be assumed close to the powder bed density. Based on this, the theoretical powder layer height h_{pow_theo} can be determined with Eq. 1 using a_p as estimation for a to

h_{pow_theo} = 43 µm / 0.54 = 79 µm. Applying Eq. *2* the increase in powder layer height h_{pow_x} due to spatter and denudation effects amounts to 112 µm. This corresponds to 58% of the total effective powder layer height h_{pow}. To rationalize those results one can calculate the resulting powder layer density for a 19 µm powder layer to consolidate to 43 µm of melted material to a = 43 µm / 191 µm = 0.23. This value is unrealistically low with a powder bed density of 0.54 and therefore powder layer density cannot solemnly account for the measured value of effective powder layer thickness.

3.3. Variation of nominal layer thickness

The resulting effective powder layer heights h_{pow} for varying nominal layer thicknesses h_n are shown in Table 4. The effective powder layer height declines with decreasing nominal layer thickness, however, the relative factor F between nominal and effective layer thickness increases as demonstrated in Fig. 7. This trend is similar for both investigated laser parameter sets, whereby the selected laser parameter set appears to influence the slope. At higher layer thicknesses this behavior seems to approach a constant factor. For the basic parameter set and nominal layer heights h_n which are equal or higher than 40 µm a factor F of 4.5 is evaluated. Because the effective melted layer heights of all samples are about equal to the adjusted nominal layer thicknesses, the effective powder layer height of small nominal layer thicknesses is higher than expected. In comparison to the basic parameter set, the measured effective powder layer thickness h_{pow} of the specimens, produced with set *L2*, are lower and therefore the values of factor F are decreased. The observed dependence on layer thickness is in accordance with results of Wischeropp et al. (2019) for 17-4 PH with effective layer thicknesses 5.5 and 4.5 times the respective nominal layer thicknesses of 30 µm and 50 µm.

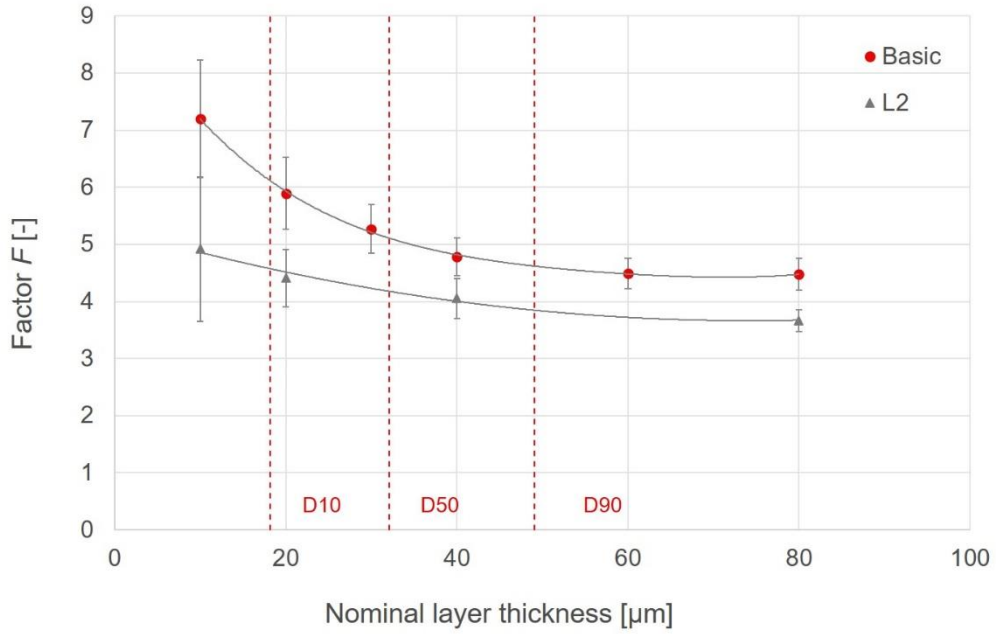

Fig. 7: Results of factor *F* between effective and nominal layer thickness for varying nominal layer thicknesses h_n = 10 µm, 20 µm, 30 µm, 40 µm, 60 µm, 80 µm (error bars represent the standard deviations)

Table 4: Values of the sample measurement with varied nominal layer thicknesses h_n = 10 µm, 20 µm, 30 µm, 40 µm, 60 µm, 80 µm and the basic parameter set and set *L2*

Nominal layer thickness h_n [µm]	Effective powder layer height h_{pow}		Effective melted layer height h_l		Factor *F*
	Height [µm]	STD [µm]	Height [µm]	STD [µm]	$\frac{h_{pow}}{h_n}$
Basic parameter set					
10	72	10	13	7	7.2
20	118	13	22	5	5.9
30	158	13	33	7	5.3
40	191	13	43	8	4.8
60	269	16	62	10	4.5
80	358	23	80	16	4.5
Set *L2*					
10	49	13	12	10	4.9
20	88	10	21	4	4.4
40	162	14	44	7	4.1
80	293	15	80	8	3.7

STD – Standard deviation

Mahmoodkhani et al. (2019) also investigated 17-4 PH and found effective layer thickness 7.5 times the nominal thickness of 20µm. The observed dependence on layer thickness is in accordance with results of Wischeropp et al. (2019) for 17-4 PH with effective layer thicknesses 5.5 and 4.5 times the respective nominal layer thicknesses of 30 µm and 50 µm. Mahmoodkhani et al. (2019) also investigated 17-4 PH and found effective layer thickness 7.5 times the nominal thickness of 20µm. Although a direct comparison of the effect of nominal layer thicknesses from those papers might not be valid due to different processing parameters used for the different nominal layer thicknesses, the results indicate a comparable trend. However, no explanation is given for the different ratios in Wischeropp et al. (2019). In the following we want to present possible explanations.

The observed trend could be explained by changing powder layer densities. Mindt et al. (2016) showed in several simulations that the powder layer density of the first layer is determined by nominal layer thickness h_n which defines the gap height between building platform and coating blade. The lower h_n is, the lower the powder layer density of the fist layer gets. At low gap heights, only small particles can be stored which is just a low percentage of total particles. However, these findings can only be applied to the first layer or the powder bed, but not the recoating of solidified material. According to the results the effective layer thickness h_{pow} of all investigated samples is higher or equal than the determined *D90* particle size and therefore a significant change in powder layer density is not expected. However, it can be assumed that in processes with lower nominal layer thicknesses the particle size in the powder section, in which the layer shift height corresponds to the nominal layer thickness, is changed. For lower gap heights only the small sized particles would be deposited in the powder bed, while larger particles would be accumulated in front of

the recoater and deposited as soon as the gap height increases over the solidified surface. Thus, a different particle size distribution could be established changing the powder layer density. Therefore, the particle size distribution was measured for powder deposited at different locations in the powder bed and upon the solidified layer and compared to the initial powder particle size distribution in the dispenser for two different nominal layer thicknesses. The outcomes of the particle size analysis for 10 µm and 80 µm nominal layer thickness is shown in Fig. 8. The analysis of the powder particle size distribution for samples taken from different locations in the powder bed show an increased deposition of smaller particles for the 10 µm process and a gradient along the recoating direction compared to the 80 µm process. A high number of smaller particles is deposited at location P3, which was samples from the powder bed between the dispenser and the part. The powder samples of location P4 are taken at a similar x-direction, which is the recoating direction, as the part. The distribution for 10 µm slightly shifts to higher values, which can be explained as less smaller particles will be available for deposition along the recoating direction. No gradient is observed for 80 µm nominal layer thickness as the gap height is higher than the *D90* of the powder particles. Despite the difference in the powder bed region there is no significant difference regarding the particle size distribution for powder

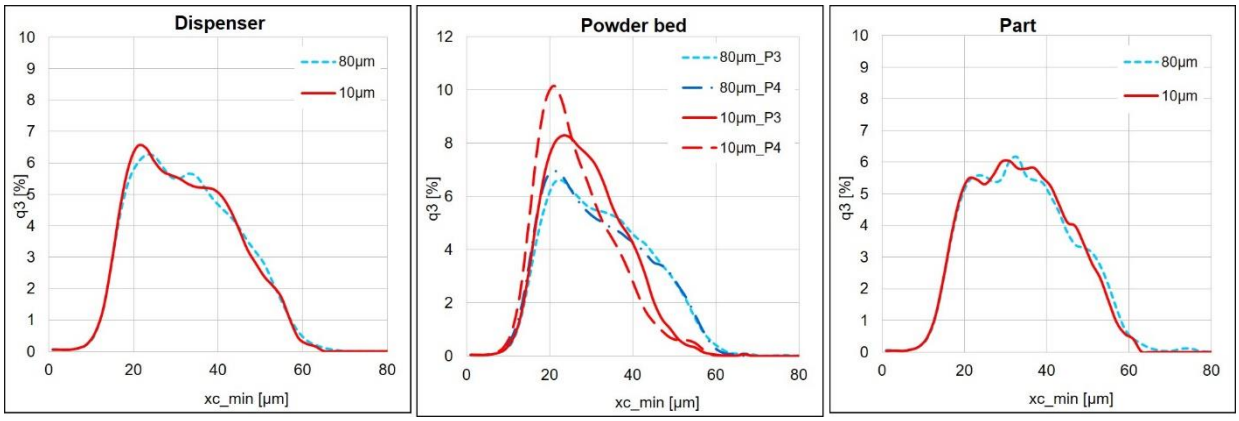

Fig. 8: Results of powder particle size distribution analysis of the building processes with 10 µm and 80 µm nominal layer thickness by evaluating different sections of the process chamber, P3: Powder bed region at similar x-direction to part, P4: Powder bed region between dispenser and part

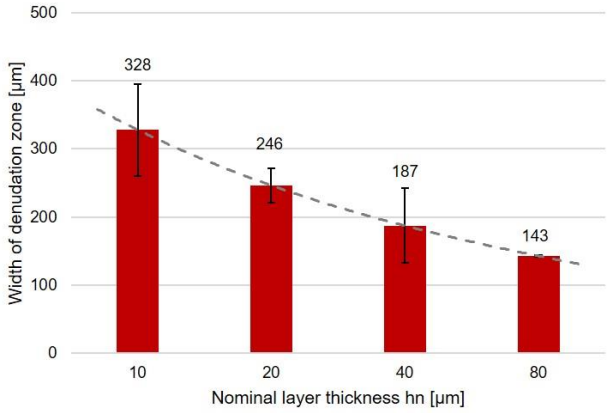

Fig. 9: Results of measuring the denudation zone width by varying nominal layer thickness h_n = 10 µm, 20 µm, 40 µm, 80 µm and basic parameter set (error bars represent the standard deviations)

lying on the generated part. Thus, the powder layer density should not change with decreasing layer thickness.

Other factors contributing to the evolution of effective layer thickness are spatter and denudation which might vary in dependence of nominal layer thickness. It must be noted that the direct examination of the influence on spattering was not possible to investigate with the available resources. However, most spatter is due to entrainment of powder particles by the vapor plume and thus related to the denudation zone (Ly et al., 2017). Fig. 9 shows the results for the influence of the nominal layer thickness on the denudation zone formation. The lower the nominal layer thickness is, the higher the width of the denudation zone gets. Thus, small nominal layer thicknesses lead to a higher denudation effect. As a result, more particles are deposited during exposure and the effective layer thickness increases. This finding fits with the received development of the effective layer height by varying the nominal layer thickness (Fig. 7). We assume that due to the higher surface quality of processes with small nominal layer thicknesses the frictional resistance is smaller, so that the powder particles can be deposited more easily during the exposure. The surface

roughness increases from 1 ± 3 µm for samples fabricated with nominal layer thickness of 10 µm to 16 ± 5 µm for 80 µm nominal layer thickness. A decrease of the denudation zone with increasing layer thickness was also observed by Bidare et al. (2018) using high speed imaging of multilayer scans. It was suggested that with higher layer thicknesses powder particles from the surrounding were more prone to roll towards the melted track filling up the denudation zone. Additionally, it was stated that surface roughness of the solidified layer could also provide a reduction in denudation compared to the first layer scanned on the comparably smoother base plate. This was deduced as the direct application of the effective layer thickness of 130 µm on the substrate plate resulted in a wider denudation zone compared to a multilayer build in steady state. For the presented experiment, it should be noted that the variation of dose factor and multiple coating have no influence on the effective powder layer height (Fig. 10). Thus, it can be assumed that the denudation results are valid for the according effective layer thicknesses despite multicoating used for the denudation samples.

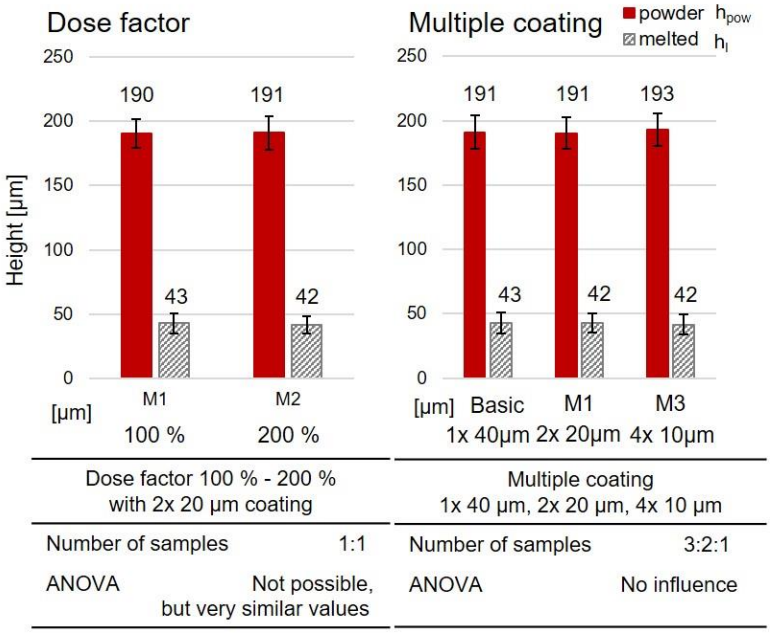

Fig. 10: Results of measurement of effective powder and melted height by variation of dose factor and multiple coating before laser exposure (error bars represent standard deviations)

3.4. Variation of laser parameter

Compared to the basic parameter set, the effective powder layer height h_{pow} of set *L1* and *L2* is lower (Fig. 11). In contrast, the effective powder layer thickness of set *L3* is sharply increased. Thus, the variation of laser parameters has a significant impact on the development of the examined value. Because the increase of powder layer height is caused by spatter and denudation effects, it is assumed that the choice of laser parameters affects the formation of these effects. For set *L1* and *L2* less powder is deposited compared to the basic parameter set during exposure. This reduces the resulting powder layer height h_{pow}. In contrast, through the exposure process with parameter set *L3* much higher powder particle deposition had occurred. Considering the findings of the denudation zone development by varying the laser parameters (Fig. 12), a similar behavior can be observed. For example, the width of the denudation zone of set *L3* is clearly larger than the value of all other parameter sets. This confirms that more powder particles are deposited during the exposure process.

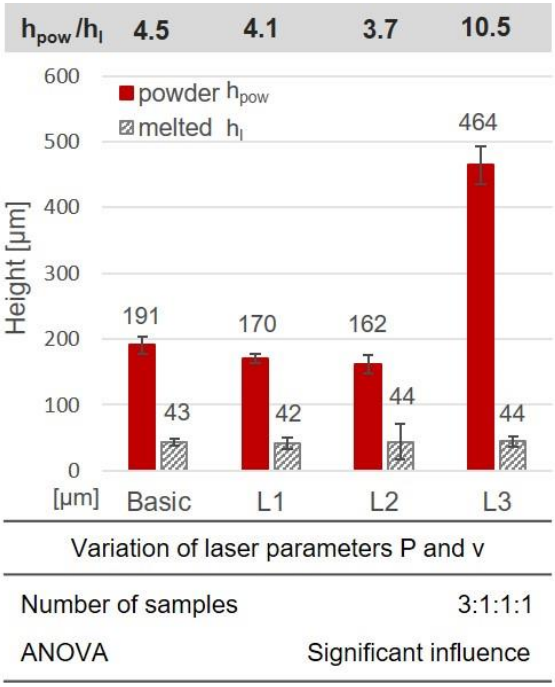

Fig. 11: Results of the measurement of effective powder and melted layer height of set *L1*, *L2* and *L3* with varied laser parameters compared to the basic parameter set in steady state (error bars represent standard deviations)

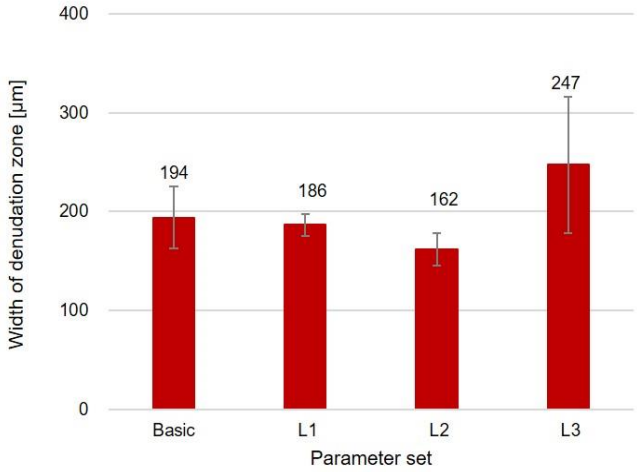

Fig. 12: Results of measuring the denudation zone width by varying laser parameter sets (error bars represent the standard deviations)

The resulting denudation zone width of the basic parameter set, set *L1* and set *L2* also fit to the obtained effective powder layer thicknesses (Fig. 11). The wider the denudation zone is, the more powder particles are deposited and the higher the effective layer thickness gets. However, the influence of spatter must be included in the general consideration, as well. According to the investigation of Matthews et al. (2016), the denudation zone expands with increasing laser power, while it is less influenced by scan speed. This observation is in accordance with the analysis of Gunenthiram et al. (2017), which measured an increased denudation zone with increasing laser power. Comparing the molten layer volume to the total powder volume within the denudation and track region they calculated an estimate of the ejected particle fraction and its dependence on laser power. A rise in laser power which equals an increase in input energy at constant scan speed results in a higher number of spatters with an increased number of larger particles. This could explain the low powder layer height of set *L1* compared to the basic parameter set as a lower laser power was used at the same scan speed. Accordingly, an increase effective powder layer height is expected for set *L3* due to the high energy input by reduction

of scan speed. However, set *L2* produced with increased laser power and decreased speed should also have a higher powder layer height than the basic samples. This is not the case. These results give a clue for explaining the different effective powder layer heights at varying laser parameters. Nevertheless, the general influence of the interaction of laser power and scan speed on spatter and denudation effect is still unknown and should be examined more closely, e.g., with high-speed-video-recordings.

3.5. Powder consumption

Table 5 shows the calculation of the increase of effective powder layer thickness of several samples. All resulting powder layer thicknesses are at least 98% higher than theoretically expected. The highest increase of approx. 465% compared to the theoretical powder layer thickness results with a nominal layer height of 40 µm and parameter set *L3*. In this context, it is especially noticeable that the variation of laser parameters has a recognizable impact on the increase of the effective powder layer thickness h_{pow_x}. With the variation of laser parameters, the increase in effective powder layer height varies within 365% from the lowest to the highest effective layer thickness. In contrast, the increase of powder layer height by varying the nominal layer thickness shows a significantly smaller span of about 24 – 55%.

Table 5: Values for calculation of the increase of effective powder layer height h_{pow_x} due to spatter and denudation effects with powder bed density a=0.54

	h_n [µm]	h_l [µm]	h_{pow} [µm]	h_{pow_theo} [µm] (= h_l/a)	h_{pow_x} [µm] (= $h_{pow} - h_{pow\_theo}$)	h_{pow_x} [%] (related to h_{pow_theo})	Max(h_{pow_x}) – Min(h_{pow_x}) [%]
Variation nominal layer thickness h_n (Basic parameter set)							
10 µm	10	13	72	25	47	191	approx. 55%
20 µm	20	22	96	40	56	140	
30 µm	30	33	158	61	97	158	
40 µm	40	43	191	79	112	141	
60 µm	60	62	269	114	155	136	
80 µm	80	80	358	148	210	141	
Variation nominal layer thickness h_n (Parameter set *L2*)							
10 µm	10	12	49	23	26	114	approx. 24%
20 µm	20	21	88	40	48	122	
40 µm	40	44	162	81	81	100	
80 µm	80	80	293	148	145	98	
Variation laser parameters *P* and *v* (constant nominal layer thickness)							
Basic	40	43	191	79	112	141	approx. 365%
L1	40	42	170	77	93	120	
L2	40	434	162	81	81	100	
L3	40	44	464	82	382	465	

4. Conclusion

Based on previous investigations, in this study the actual powder layer height in DMLS process was measured and investigated by variation of nominal layer thicknesses and laser parameters. The following new findings of the effective powder layer thickness were elaborated:

1. The variation of the laser parameters has a significant impact on the formation of effective powder layer height because of spatter and denudation effects. It is therefore recommended to consider the powder consumption when evaluating and optimizing new parameter sets. A similar setup to the denudation experiments described in this paper could be used as a first estimation of powder consumption for new process parameters as it is fast and easy to perform and showed good qualitative agreement with the effective powder layer thickness trends.
2. The factor describing the ratio between the effective and nominal layer thickness rises with decreasing nominal layer height. Thus, the height of the effective layer thickness is relatively higher using low nominal layer thicknesses. Moreover, the slope of this development seems to depend on the selected laser parameter set. For the investigated material it is therefore recommended to use a nominal layer thickness above 30 µm to decrease powder consumption. In case, a lower nominal layer thickness is necessary, e.g. loss in geometrical accuracy due to the staircase effect, process parameters could be adjusted as stated in 1. Furthermore, a variation of nominal layer thicknesses within one component to only build critical areas with small nominal layer thicknesses would be beneficial in terms of powder consumption in addition to build time savings. This is an

important aspect not considered so far for components build with varied nominal layer thicknesses.

3. The denudation effect is amplified at low layer thicknesses. This might be a result of the higher surface finish which leads to a reduced frictional resistance and thus to a support of the powder deposition.
4. By considering the used parameter sets, powder consumption increases to 98 - 465% than theoretically expected.

This study and its findings are important for an improved modelling and simulation of the melting process and dynamics in selective laser melting. Furthermore, it gives indications that will help to understand and explain the increased powder consumption during the building process. However, the formation of denudation zone and of spatter by varying process parameters and their influence on the effective powder layer height require further investigations (e.g high-speed-video-recordings).

Declaration of interests

The authors declare that they have no known competing financial interests or personal relationships that could have appeared to influence the work reported in this paper.

Funding

This research did not receive any specific grant from funding agencies in the public, commercial, or not-for-profit sectors.

References

Ali, U., Mahmoodkhani, Y., Shahabad, S. I., Esmaeilizadeh, R., Liravi, F., Sheydaeian, E., Huang, K. Y., Marzbanrad, E., Vlasea, M., Toyserkani, E., 2018. On the measurement of relative powder-bed compaction density in powder-bed additive manufacturing processes. Mater. Des. 155 495-501. DOI: 10.1016/j.matdes.2018.06.030

Bidare, P., Maier, R.R.J., Beck, R.J., Shephard, J.D., Moore, A.J., 2017. An open-architecture metal powder bed fusion system for in-situ process measurements. Addit. Manuf. 16, 177-185. DOI: 10.1016/j.addma.2017.06.007

Bidare, P., Bitharas, I., Ward, R.M., Attallah, M.M., Moore, A.J., 2018. Fluid and particle dynamics in laser powder bed fusion. Acta Mater. 142, 107-120. DOI: 10.1016/j.actamat.2017.09.051

De Souza, A.F., Al-Rubaie, K.S., Marques, S., Zluhan, B., Santos, E.C., 2019. Effect of laser speed, layer thickness, and part position on the mechanical properties of maraging 300 parts manufactured by selective laser melting. Mater. Sci. Eng. A 767, 138425. DOI: 10.1016/j.msea.2019.138425

EOS GmbH – Electro Optical Systems, 2011. EOS NickelAlloy IN718. Material data sheet. Ed. 10.2011, Munich.

Gebhardt, A., Hötter, J.-S., 2016. Additive manufacturing: 3D printing for prototyping and manufacturing, Hanser Publications, Cincinnati.

Gunenthiram, V., Peyre, P., Schneider, M. Dal, M., Coste, F., Fabbro, R., 2017. Analysis of laser-melt pool-powder bed interaction during the selective laser melting of a stainless steel. J. Laser Appl. 29, 022303. DOI: 10.2351/1.4983259

International Organization for Standardization, 2004. Lasers and laser-related equipment — Test methods for laser beam widths, divergence angles and beam propagation ratios — Part 3: Intrinsic and geometrical laser beam classification, propagation and details of test methods (ISO/TR 11146-3:2004-02(E)), Geneva.

Karapatis, N.P., Egger, G., Gygax, P.E., Glardon, R., 1999. Optimization of powder layer density in selective laser sintering. Proceedings of the International Solid Freeform Fabrication Symposium, Austin, USA, 255-263.

Kurzlechner, Q., 2016. Untersuchung des Einflusses von Beschichtungssystemen auf die Pulverbettdichte von Metallpulver in der Additiven Fertigung. Bachelor Thesis. Hochschule Landshut, Landshut.

Leicht, A., Fischer, M. Klement, U., Nyborg, L., Hryha, E., 2021. Increasing the

Productivity of Laser Powder Bed Fusion for Stainless Steel 316L through Increased Layer Thickness. J. Mater. Eng. Perform. 30, 575-584. DOI: 10.1007/s11665-020-05334-3

Li, R., Liu, J., Shi, Y., Wang, L. Jiang, W.,2012. Balling behavior of stainless steel and nickel powder during selective laser melting process. Int. J. Adv. Manuf. Technol. 59, 1025-1035. DOI: 10.1007/s00170-011-3566-1

Ly, S., Rubenchik, A.M., Khairallah, S.A., Guss, G., Matthews, M.J., 2017. Metal vapor micro-jet controls material redistribution in laser powder bed fusion additive manufacturing. Sci. Rep. 7, 1-12. DOI: 10.1038/s41598-017-04237-z

Ma, M., Wang, Z., Gao, M., Zeng, X., 2015. Layer thickness dependence of performance in high-power selective laser melting of 1Cr18Ni9Ti stainless steel. J. Mater. Process Technol. 215, 142-150. DOI: 10.1016/j.jmatprotec.2014.07.034

Mahmoodkhani, Y., Ali, U., Shahabad, S. I., Kasinathan, A. R., Esmaeilizadeh, R., Marzbanrad, E., Toyserkani, E., 2019. On the measurement of effective powder layer thickness in laser powder-bed fusion additive manufacturing of metals. Progr. Addit. Manuf. 4, 109-116. DOI: 10.1007/s40964-018-0064-0

Matthews, M. J., Guss, G., Khairallah, S. A., Rubenchik, A. M., Depond, P. J., King, W. E., 2016: Denudation of metal powder layers in laser powder bed fusion processes. Acta Mater. 114, 33-42. DOI: 10.1016/j.actamat.2016.05.017

Meiners, W., 1999. Direktes selektives Laser Sintern einkomponentiger metallischer Werkstoffe. Doctoral thesis. Shaker Verlag (Berichte aus der Lasertechnik), Aachen. ISBN: 3-8265-6571-1

Mindt, H. W., Megahed, M., Lavery, N. P., Holmes, M. A., Brown, S. G. R., 2016. Powder Bed Layer Characteristics: The Overseen First-Order Process Input. Metall. Mater. Trans. A. 47, 3811-3822. DOI: 10.1007/s11661-016-3470-2

Nguyen, Q.B., Luu, D.N., Nai, S.M.L., Zhu, Z., Chen, Z., Wei, J., 2018. The role of powder layer thickness on the quality of SLM printed parts. Arch. Civ. Mech. Eng. 18, 948-955. DOI: 10.1016/j.acme.2018.01.015

Shamsdini, S., Shakerin, S., Hadadzadeh, A., Amirkhiz, B.S., Mohammadi, M., 2020. A trade-off between powder layer thickness and mechanical properties in additively manufactured maraging steels. Mater. Sci. Eng. A 776, 139041. DOI: 10.1016/j.msea.2020.139041

Spierings, A.B., Levy, G., 2009. Comparison of density of stainless steel 316L parts produced with selective laser melting using different powder grades. Proceedings of the Annual International Solid Freeform Fabrication Symposium, Austin, USA, 342-353.

Sufiiarov, V.S., Popovich, A.A., Borisov, E.V., Polozov, I.A., Masaylo, D.V., Orlov, A.V., 2017. The effect of layer thickness at selective laser melting. Procedia Eng. 174, 126-134. DOI: 10.1016/j.proeng.2017.01.179

Vock, S., Klöden, B., Kirchner, A., Weißgärber, T., Kieback, B., 2019. Powders for powder bed fusion: a review. Progr. Addit. Manuf. 4, 383-397. DOI: 10.1007/s40964-019-00078-6

Wischeropp, T. M., Emmelmann, C., Brandt, M., Pateras, A., 2019. Measurement of actual powder layer height and packing density in a single layer in selective laser melting. Addit. Manuf. 28, 176-183. DOI: 10.1016/j.addma.2019.04.019

Yadroitsev, I., Smurov, I., 2010. Selective laser melting technology: from the single laser melted track stability to 3D parts of complex shape. Phys. Procedia. 5, 551-560. DOI: 10.1016/j.phpro.2010.08.083

Yang, J., Han, J., Yu, H., Yin, J., Gao, M., Wang, Z., Zeng, X., 2016. Role of molten pool mode on formability, microstructure and mechanical properties of selective laser melted Ti-6Al-4V alloy. Mater. Des. 110, 558-570. DOI: 10.1016/j.matdes.2016.08.036

Figure and Table Captions